Computers and Geotechnics 71 (2016) 30–46

Contents lists available at ScienceDirect

Computers and Geotechnics

journal homepage: www.elsevier.com/locate/compgeo

Review

Benchmarking the numerical Discontinuous Deformation Analysis method

Gony Yagoda-Biran *, Yossef H. Hatzor

Department of Geological and Environmental Sciences, Ben-Gurion University of the Negev, P.O. Box 653, Be'er-Sheva 84105, Israel

ARTICLE INFO

Article history:
Received 11 September 2014
Received in revised form 19 April 2015
Accepted 23 August 2015

Keywords:
Discontinuous Deformation Analysis
Benchmark tests
Verification
Validation
Dynamic analysis

ABSTRACT

The Discontinuous Deformation Analysis (DDA) method is an important tool for investigating the dynamics of systems composed of multiple discrete elements such as masonry structures and blocky rock masses. As such it has become a popular investigative tool in geotechnical and rock engineering research. In this paper dynamic verification studies of 2D and 3D-DDA performed by the rock mechanics research group at the Ben-Gurion University of the Negev, Israel (BGU), are reviewed. The analytical verifications developed and reviewed here allow critical assessment of the advantages and limitations of 2D and 3D-DDA, can be used as benchmark tests for attempted modifications to the original DDA code, for calibration of input numerical control parameters, and for quantitative and meaningful comparison with other numerical discrete element methods.

Contents

* Corresponding author at: Geological Survey of Israel, 30 Malkhe Israel St., Jerusalem 95501, Israel.
E-mail address: gonyb@gsi.gov.il (G. Yagoda-Biran).

http://dx.doi.org/10.1016/j.compgeo.2015.08.003
0266-352X/

1. Introduction

Discontinuous Deformation Analysis (DDA) is an implicit, discrete element method proposed by Shi [1–4] to provide a tool useful for investigating the dynamics of blocky rock masses and systems composed of multiple blocks. The 2D-DDA was proposed first, at the 1980s at UC Berkeley, and the 3D-DDA was published later [5]. A good review of the essentials of DDA is provided by Jing [6]. Reviews of DDA within the scope of other numerical methods used today to solve problems in rock mechanics and rock engineering are provided by Jing [7], Jing and Hudson [8] and Jing and Stephansson [9]. Many verification and validation studies have been performed to test the capability of DDA to solve static as well as dynamic problems since its publication. A comprehensive review of 2D-DDA validations is provided by MacLaughlin and Doolin [10]. The 3D-DDA, being a more recent development, has not been verified extensively and this paper presents new and useful validations also of 3D-DDA.

Many research groups have made modifications to the original code developed by Shi [1,3,4] in an attempt to better address some of the fundamental issues in DDA. For example, Lin et al. [11] modified the original contact model of DDA, which is based on the penalty method, by adopting the Lagrange type approach. Ning et al. [12] modified the contact algorithm of DDA by adopting the Augmented Lagrangian method. Bao and Zhao [13,14] have made some enhancements to the vertex to vertex contact. In an attempt to overcome the DDA simply deformable blocks assumption and therefore uniform distribution of stresses within blocks, Shi [15] developed the Numerical Manifold Method, using superposition of a mathematical cover over the physical mesh of the blocks. Bao and Zhao [16] have integrated the advantages of both DDA and the finite element methods (FEM), and developed the hybrid nodal-DDA (NDDA), thus improving the accuracy of stress distribution and allowing for crack propagation within blocks. Jiao et al. [17] developed a two-dimensional contact constitutive model to simulate the fragmentation of jointed rock. Several other research groups have developed higher order DDA codes to address this issue e.g. [18]. Jiao et al. [19] applied a viscous boundary in DDA based on the standard viscous boundary condition provided in the original DDA formulation, in order to deal with dynamic wave propagation problems. Later on Bao et al. [20] implemented new viscous boundary conditions to the 2D-DDA, in order to improve the absorbing efficiency. Mikola and Sitar [21] developed a 3D-DDA formulation using an explicit time integration procedure, and a different contact detection algorithm. Kim et al. [22] and Jing et al. [23] have made a modification where they compute water pressure and seepage through rock mass, this way coupling fluid flow in fractures. More recent implementations of hydro-mechanical coupling in DDA was developed by Chen et al. [24] and Ben et al. [25]. Koyama et al. [26] combined the DDA and the finite element method for fluid flow simulation to model the interaction between solid particles movement and fluid flow. Wu et al. [27] developed a post-contact adjustment method to overcome issues when addressing rock fall problems in the original code. A model for cable bolt–rock mass interaction was integrated with DDA by Moosavi and Grayeli [28]. Other useful developments and applications of DDA are summarized in a series of ICADD proceedings (International Conference on Analysis of Discontinuous Deformation) published biannually since 1995.

In this paper we review illustrative benchmark tests performed by members of the rock mechanics group at the Ben-Gurion University of the Negev (BGU), with the original codes of 2D and 3D-DDA. These tests could be performed in every development of the DDA code, for verification purposes. We compare all benchmark tests reported here with analytical solutions, some developed at BGU and some adopted from existing publications. The authors do acknowledge other verification studies performed by other research groups, such as the extensive study of sliding blocks performed at Nanyang Technological University in Singapore [29], slope stability kinematics [30] and analysis of three-hinged beams [31] performed at U.C. Berkeley, and more, but here only verifications resulting from BGU research are discussed, for brevity. Verifications that have already been published are briefly summarized. New verifications that have never been published are presented more thoroughly.

We begin with a brief summary of DDA fundamentals in Section 2, followed by review of published verifications of 2D-DDA in Section 3, and presentation of published and newly developed results of 3D-DDA in Section 4. Summary of results and conclusions are presented in Section 5.

2. DDA fundamentals

DDA considers both statics and dynamics using a time-step marching scheme and an implicit algorithm formulation. The static analysis assumes the velocity of the different block elements is zero at the beginning of each time step, while the dynamic analysis assumes the velocity at the beginning of a time step is inherited from the previous one. The criterion for convergence in DDA is that there will be neither tension nor penetration between the blocks. These two constraints are applied using a penalty method, where stiff springs are attached to the contacts. Extension or compression of the springs are energy consuming, therefore the minimum energy solution utilized in DDA assures no penetration or tension between the blocks.

In the original code of the DDA, a damping submatrix was not incorporated in the equilibrium equations. There are two ways to introduce damping in the original code: the time step marching

scheme introduces algorithmic damping [32], that is determined by the time step size used, and will be briefly discussed later, and kinetic damping. The latter can be applied by assigning a number lower than 1 for the dynamic control parameter: a value of zero means the analysis is static and the velocity is zeroed at the beginning of each time step, a value of unity means the analysis is fully dynamic and the velocity at the beginning of a time step is inherited from the previous one, and any value between zero and one corresponds to the percentage of the velocity that is inherited from one time step to the next. For example, a value of 0.98 corresponds to 2% kinetic damping.

In this section the basic equations of the 2D-DDA will be briefly reviewed. The 3D-DDA shares the same basic principles, extended to 3D. In the DDA method the simultaneous equilibrium equations, which are derived by minimizing the total potential energy of the system, Π, are written as:

$$\mathbf{M}\ddot{\mathbf{d}} + \mathbf{C}\dot{\mathbf{d}} + \mathbf{K}\mathbf{d} = \mathbf{f} \tag{1}$$

M, **C**, and **K** are the mass, damping, and stiffness matrices, respectively, and **d** and **f** are the displacement unknowns and force vectors. In a two-dimensional DDA model with n blocks, the basic element is a block with six unknowns:

$$\mathbf{d}_i = \{\, u_0 \quad v_0 \quad r_0 \quad \varepsilon_x \quad \varepsilon_y \quad \gamma_{xy} \,\}_i^T, \quad (i = 1, 2, \ldots, n) \tag{2}$$

where (u_0, v_0) are the rigid body translations, r_0 is the rotation angle of the block with respect to the rotation center at (x_0, y_0), and ε_x, ε_y and γ_{xy} are the normal and shear strains of the block. As shown by Shi [3], the complete first order approximation of displacements at any point (x, y) takes the following form:

$$\begin{Bmatrix} u_x \\ u_y \end{Bmatrix}_i = \mathbf{T}_i \mathbf{d}_i, \quad (i = 1, 2, \ldots, n) \tag{3}$$

where

$$\mathbf{T}_i = \begin{bmatrix} 1 & 0 & -(y - y_0) & (x - x_0) & 0 & \frac{(y-y_0)}{2} \\ 0 & 1 & (x - x_0) & 0 & (y - y_0) & \frac{(x-x_0)}{2} \end{bmatrix}_i \tag{4}$$

By adopting first order displacement approximation, the distribution of the stresses and strains is constant within a block.

Assuming the velocity at the beginning of the time step, which can be obtained from the previous time step, is $\dot{\mathbf{d}}_0$, and that the time interval of a single time step is Δ, then:

$$\begin{aligned} \ddot{\mathbf{d}} &= \frac{2}{\Delta^2}(\mathbf{d} - t\dot{\mathbf{d}}_0), \\ \dot{\mathbf{d}} &= \frac{2}{\Delta}\mathbf{d} - \dot{\mathbf{d}}_0 \end{aligned} \tag{5}$$

By substituting Eqs. (5) into (1) the simultaneous equilibrium equations can be rewritten as:

$$\hat{\mathbf{K}}\mathbf{d} = \mathbf{f} \tag{6}$$

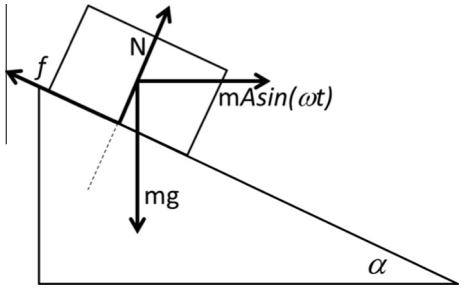

Fig. 1. Schematics of the block on an inclined plane problem.

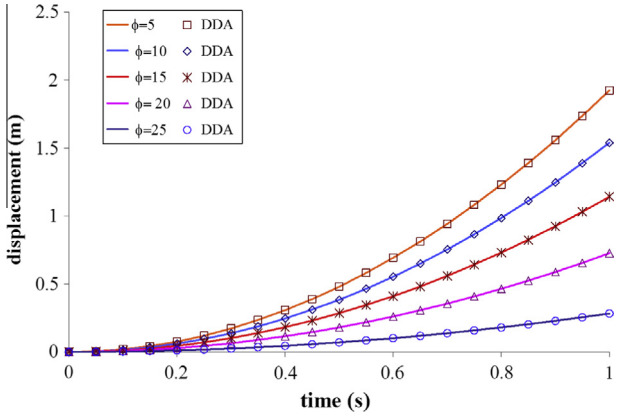

Fig. 2. Block displacement vs. time for the case of a block on an incline – gravitational loading only. Comparison between analytical (lines) and DDA (symbols) solutions, as computed by Kamai [35], after MacLaughlin [36].

where $\hat{\mathbf{K}}$ is the equivalent global stiffness matrix. Eq. (6) can be written in a sub-matrix form as follows:

$$\begin{bmatrix} \mathbf{K}_{11} & \mathbf{K}_{12} & \mathbf{K}_{13} & \cdots & \mathbf{K}_{1n} \\ \mathbf{K}_{21} & \mathbf{K}_{22} & \mathbf{K}_{23} & \cdots & \mathbf{K}_{2n} \\ \mathbf{K}_{31} & \mathbf{K}_{32} & \mathbf{K}_{33} & \cdots & \mathbf{K}_{3n} \\ \vdots & \vdots & \vdots & \ddots & \vdots \\ \mathbf{K}_{n1} & \mathbf{K}_{n2} & \mathbf{K}_{n3} & \cdots & \mathbf{K}_{nn} \end{bmatrix} \begin{Bmatrix} \mathbf{d}_1 \\ \mathbf{d}_2 \\ \mathbf{d}_3 \\ \vdots \\ \mathbf{d}_n \end{Bmatrix} = \begin{Bmatrix} \mathbf{f}_1 \\ \mathbf{f}_2 \\ \mathbf{f}_3 \\ \vdots \\ \mathbf{f}_n \end{Bmatrix} \tag{7}$$

where $\mathbf{K}_{ij}(i, j = 1, 2, \ldots, n)$ are 6×6 sub-matrices; $\mathbf{d}_i$ and $\mathbf{f}_i(i = 1, 2, \ldots, n)$ are 6×1 sub-matrices corresponding to block i. For more details the interested reader is encouraged to refer to basic DDA Refs. [1,3,4].

3. Benchmark tests for dynamic 2D-DDA

In this section we will review verification studies of 2D-DDA, performed by the Rock Mechanics research group at the Ben-Gurion University of the Negev.

3.1. Block sliding on an inclined plane

A block sliding on an inclined plane is a classic problem in rock mechanics, as it is a simple and intuitive model for some cases of rock slopes, and has a straightforward analytical solution. The DDA has been verified by several researchers with the analytical solution for a block on an inclined plane. Tsesarsky et al. [33] and Kamai and Hatzor [34] have verified the 2D-DDA with the analytical solution. Ning and Zhao [29] have verified the 2D-DDA for a block sliding on an inclined plane under horizontal and vertical accelerations, and under different mechanisms of loading. In this subsection the analytical solution for a block on an incline is briefly reviewed, and the results of former verification studies of the 2D-DDA are presented.

3.1.1. Analytical solution

The model of a block on an inclined plane is presented in Fig. 1. The inclination angle of the slope is α, and the friction angle of the sliding interface is ϕ. The forces acting on the block are its self-weight mg, the normal from the plane N and the frictional force at the interface between the block and the plane, f. In the most generalized case, where an external force is applied on the block in the form of a harmonic function (Fig. 1), the downslope displacements of the block can be calculated by:

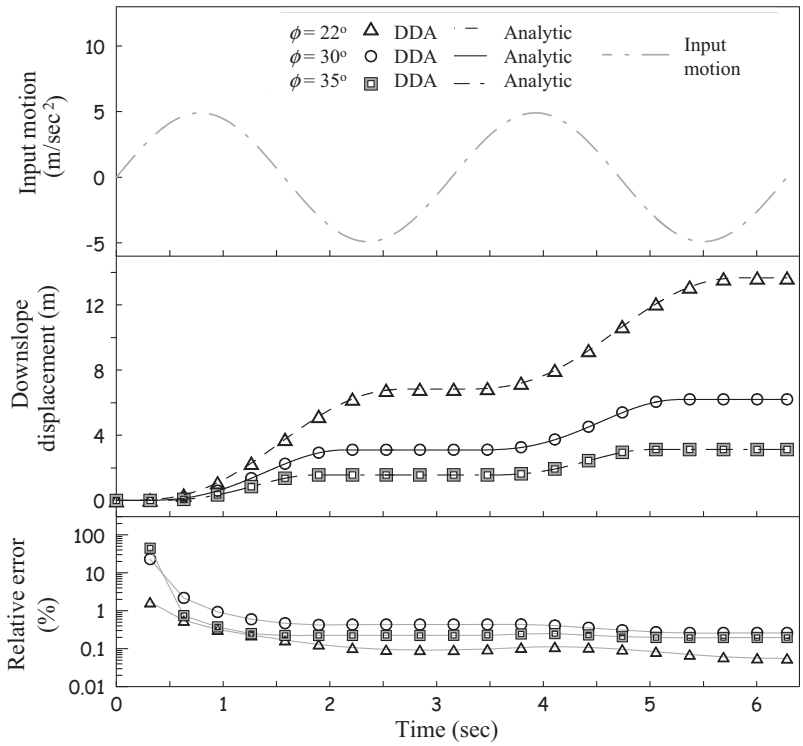

Fig. 3. Verification of the dynamic case of a block on an incline for three different interface friction angles: top—input acceleration function; center—comparison between analytical (solid line) and DDA (symbols) solutions; and bottom—relative error for each simulation. After [34].

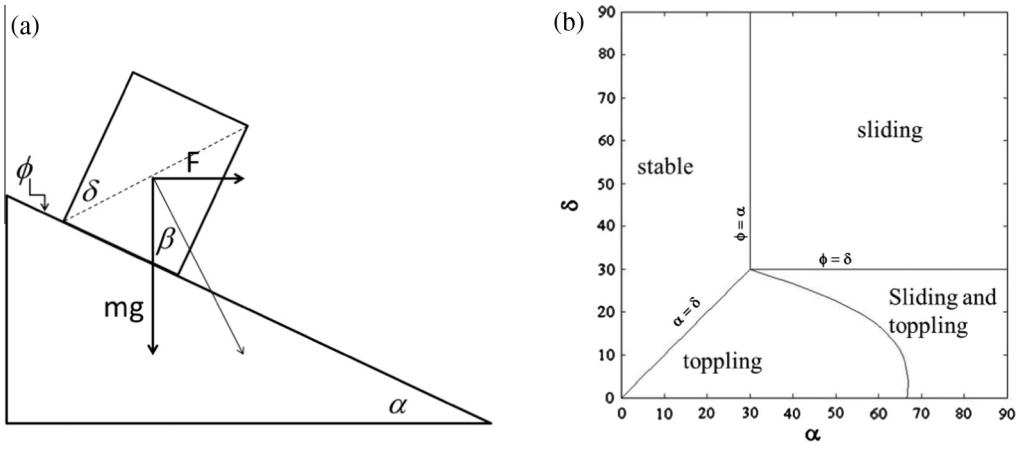

Fig. 4. (a) Schematics of the block on an incline and the angles controlling its mode. (b) An example for the failure mode chart for gravitational loading, at $\phi = 30°$. After [43].

$$d(t) = \frac{1}{2}g(\sin\alpha - \cos\alpha\tan\phi)t^2 - \frac{A}{\omega^2}\sin(\omega t)(\cos\alpha + \sin\alpha\tan\phi) + \dot{d}_0 t + d_0 \quad (8)$$

where g is the acceleration of gravity, $\tan\phi$ is the friction coefficient of the sliding interface, A and ω are the amplitude and angular frequency of the harmonic input acceleration, respectively, $\dot{d}_0$ is the initial velocity of the sliding block and d_0 is its initial displacement.

3.1.2. Block sliding on an incline with 2D-DDA

Kamai [35] performed a verification study of a block sliding on an inclined plane subjected to gravity ($A = 0$), starting at rest ($\dot{d}_0 = 0, d_0 = 0$), for an inclination angle of $\alpha = 28°$, and five different values of friction angle ϕ: 5°, 10°, 15°, 20° and 25°. She obtained a good agreement between the two solutions (Fig. 2), demonstrated by the relative numeric error, E_N:

$$E_N = \left|\frac{d_A - d_N}{d_A}\right| \cdot 100\% \quad (9)$$

where d_A and d_N are the analytical and numerical displacements, respectively. She found that the relative numeric error increases with increasing friction angle, and was lower than 8% for $\phi = 25°$, and at the order of 0.05% for $\phi = 5°$.

Kamai and Hatzor [34] then proceeded to loading the block with a sinusoidal horizontal acceleration, as in Fig. 1. In this case, downslope sliding will initiate only when the yield acceleration, $a_y = g\tan(\phi - \alpha)$, is exceeded, at time $\theta = \sin^{-1}(\tan(\phi - \alpha)g/A) * (1/\omega)$, a model proposed by Newmark [37] and Goodman and Seed

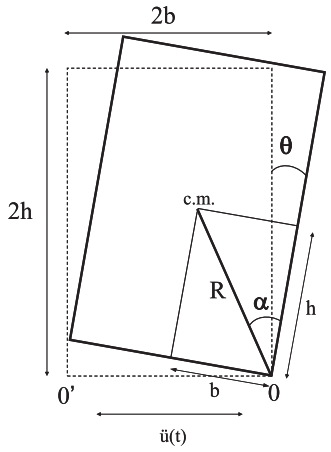

Fig. 5. Free body diagram and sign convention used in this paper for the rocking block problem.

[38], and today largely referred to as 'Newmark type' analysis. In this case, Eq. (8) becomes (assuming that $d(\theta) = \dot{d}(\theta) = 0$):

$$d(t) = g\lfloor(\sin\alpha - \cos\alpha\tan\phi)(1/2t^2 - \theta t + 1/2\theta^2)\rfloor + \frac{A}{\omega^2} \times [(\cos\alpha + \sin\alpha\tan\phi)(\omega\cos(\omega\theta)(t-\theta) - \sin(\omega t) + \sin(\omega\theta))] \quad (10)$$

The downslope displacements, $d(t)$, are calculated while a_y is exceeded for the first time at θ_1, or the block's velocity is positive. If neither condition is fulfilled, the block is at rest, and will initiate sliding only once a_y is exceeded again, at θ_2, and so on.

Kamai and Hatzor [34] have used this solution to verify the 2D-DDA. The inclination angle they used for the slope was $\alpha = 20°$, with friction angles of 22°, 30° and 35°. They obtained an excellent agreement between the analytical and numerical solutions, with relative numerical error lower than 1% for most of the simulation time (Fig. 3).

3.2. Failure mode mapping for the block on an incline problem

A block on an incline, of which sliding failure was reviewed in Section 3.1, has actually four possible modes: it can stay at rest, it can slide, it can topple, or it can slide and topple simultaneously. The actual failure mode is controlled by three factors, when the block is subjected to gravity: the inclination of the slope α, the slenderness of the block δ, and the friction angle of the interface, ϕ (see Fig. 4a). The boundaries between the modes were modified over the years [39–42] (see Fig. 4b), and recently mapping the failure mode when the block is subjected to an external pseudo-static earthquake inertia force F (see Fig. 4a), has been demonstrated [43]. Yagoda-Biran and Hatzor [43] have found that when adding a horizontal pseudo-static force, with its resultant with the weight vector forming an angle β with the vertical direction (see Fig. 4a), the mode of the block is now controlled by the slenderness of the block δ, the friction angle of the interface ϕ, and a new angle $\psi = \alpha + \beta$, rather than α.

3.2.1. Failure mode chart with 2D-DDA

The first comparison between 2D-DDA and analytically derived failure mode chart for toppling and sliding was performed by Yeung [42] at U.C. Berkeley, and the results are discussed extensively in his PhD dissertation. A brief review of Yeung's results is provided in [43]. Yeung compared the nature of the first motion of the block as computed with 2D-DDA, to the failure mode predicted by the analytical solution that was universally accepted at those days [39–41]. Yeung found that in some cases with the 2D-DDA he obtained toppling mode when he should have obtained sliding and toppling, according to the analytical solution. This observation led him to develop a new equation for the boundary between toppling and sliding and toppling. After making that modification to the boundary and turning it from static to dynamic in nature, he got a very good agreement between the 2D-DDA and the analytical solution. The agreement can't be discussed in terms of relative error, since in this case only the first motion of the block is of interest, so the degree of agreement can be thought of as binary – either the solutions agree, or they don't.

3.2.2. Comparison between 2D-DDA and modified failure mode chart under pseudo-static loading

Yagoda-Biran and Hatzor [43] used the 2D-DDA to verify their newly developed failure mode chart when a pseudo-static inertia force is also considered. They put forth a set of rules to determine the first motion of the block as obtained with DDA, and compared it to the prediction of their modified mode chart. The regions close to the boundaries were examined more thoroughly than those far

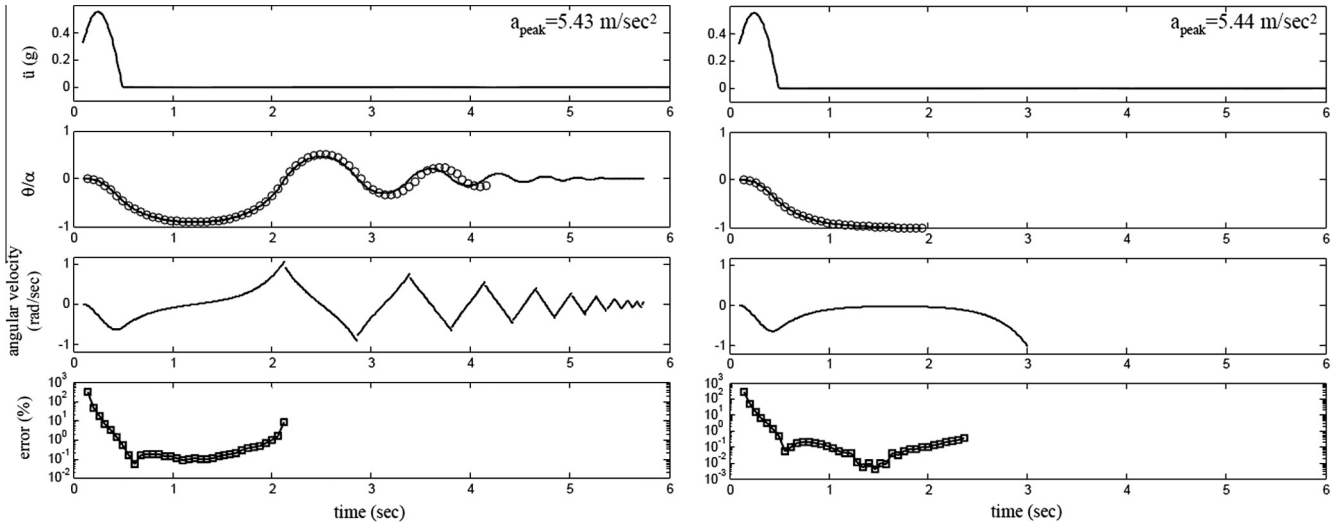

Fig. 6. Solution for dynamic column rotation ($b = 0.2$ m, $h = 0.6$ m). Left: input amplitude lower than required to topple the column, right: input amplitude sufficient for toppling. Solid line: analytical solution, open circles: DDA. From [47].

Fig. 7. The model used in the 2D verification of block response to induced displacements (after [34]).

away from the boundaries between modes. The slope angle α used was 10° for most of the simulations. The range of block slenderness δ was between 6° and 70°, and of the friction angle ϕ was 10° and 80°. The change in the angle ψ was controlled by changing the magnitude of the applied pseudo-static force. An excellent agreement was obtained between the two solutions, with the DDA returning the modes as predicted by the analytical mode chart for 106 out of the 110 simulations.

3.3. Rocking of a single block

Makris and Roussos [44] studied the problem of the dynamic rocking of a free-standing column subjected to a sinusoidal input acceleration and their analytical solution can be reviewed in [44,45]. The free body diagram for the problem is shown in Fig. 5. The analytical solution assumes that no sliding occurs at the base of the rocking block.

Yagoda-Biran and Hatzor [45] compared between results from 2D-DDA simulations and the Makris and Roussos [44] solution. They selected a geometry of a block where $b = 0.2$ and $h = 0.6$ m, and used an acceleration input function of the form $\ddot{u}_g(t) = a_p \sin(\omega_p t + \psi)$, with changing amplitude a_p and $\omega = 2\pi$ from $t = 0$ to $t = 0.5$ s. For this specific geometry and frequency of motion, the analytical solution shows that the block will not topple with $a_p = 5.43$ m/s^2, but will topple with $a_p = 5.44$ m/s^2. Yagoda-Biran and Hatzor [45] found the value of contact spring stiffness (i.e. the optimal penalty parameter) that will give the same results, in terms of stability-failure, in the 2D-DDA, and then compared the rotation time histories of the column calculated by the analytical and DDA solutions. They obtained an excellent agreement between the two solutions, where the relative error drops below 10% after about 0.3 s of simulation, and below 1% after about 0.5 s (Fig. 6). Yagoda-Biran and Hatzor [45] found that the error grows larger and the DDA deviates from the analytical solution as soon as the first impact between the rocking column and the fixed base occurs. They explained it by the way damping is implemented in the two solutions. While in the analytical solution the motion during impact is energetically damped due to conservation of angular momentum following the constant value of the coefficient of restitution [44], in DDA oscillations at contact points are restrained due to inherent algorithmic damping [32,46].

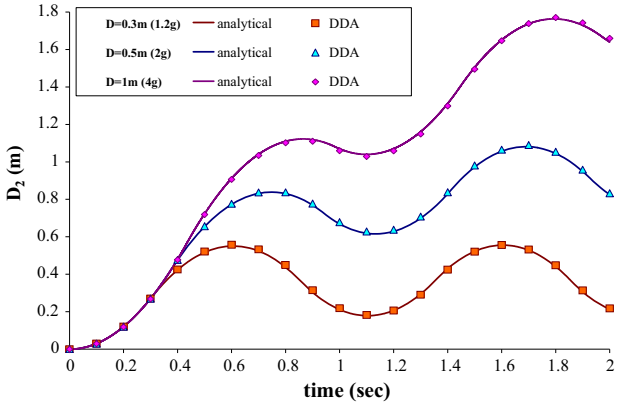

Fig. 8. Response of Block 2 to displacement input of $f = 1$ Hz. Comparison between analytical (line) and DDA (symbols) solutions for different amplitudes of motion. After [34].

3.4. Block response to shaking foundations

In the preceding discussion the dynamic response of the blocks was a result of direct dynamic input to the blocks centroid. In the case presented in this section, Kamai and Hatzor [34] verified the 2D-DDA with a semi-analytical solution for a block responding to induced displacements at its foundation. Such an application would be suitable for dynamic analysis of structures which respond to earthquake motions at their foundations. The model comprises of three blocks as follows (Fig. 7): a stationary base block (0), an intermediate block (1) to which the input displacements are applied, and an overlying very flat block (2) which responds to the induced displacements in Block 1.

Block 1 is subjected to a horizontal displacement input function in the form of a cosine, starting from zero:

$$d(t) = D(1 - \cos(2\pi f t)) \tag{11}$$

The only force acting on Block 2, other than its weight and the normal from Block 1, is the frictional force, which determines the acceleration of block 2:

$$\ddot{d}_2 = \mu g \tag{12}$$

where μ is the friction coefficient (for full derivation of equations please refer to Kamai and Hatzor [34]). The direction of the driving force is determined by the direction of the relative velocity between Block 1 and 2, denoted as $\dot{d}^*$:

$$\dot{d}^* = \dot{d}_1 - \dot{d}_2 \tag{13}$$

Kamai and Hatzor [34] defined a set of inequalities and boundary conditions that determine the magnitude and direction of the acceleration of Block 2, as a function of the acceleration of block 1 and the relative velocity between the blocks. The complete set of inequalities can be reviewed in their paper, or an equivalent set can be viewed later on in this paper.

Kamai and Hatzor [34] compared the displacements computed with 2D-DDA and the analytical solution for changing values of friction angle of the interface between blocks 1 and 2, and for changing amplitudes of input displacement. They found that generally the relative numeric error stayed below 5%, and was more sensitive to friction coefficient than amplitude changes [34]. The response of block 2 to changing amplitudes is presented in Fig. 8.

3.5. Shear wave propagation

Bao et al. [48] tested the ability of the 2D-DDA to correctly simulate wave propagation. They modeled a set of stacked horizontal layers (Fig. 9a), generated a shear wave by inducing horizontal movements at the base (Fig. 9b), and compared the waveforms at measurement point M1 in the model (Fig. 9a). Because the DDA blocks are linear elastic and un-damped, the analytical amplitude in the tests is the same amplitude as that of the incident wave at the rigid base. After performing sensitivity analysis to the block size and time step size, they managed to successfully preserve the wave form in the DDA model (Fig. 9c).

Bao et al. [48] also validated the DDA with SHAKE program for site response applications. SHAKE [49,50] is a program that analyzes the 1-dimensional response of a stack of linear-elastic layers in the frequency domain. The stack can be composed of several layers with varying properties, and it is subjected to seismic motion

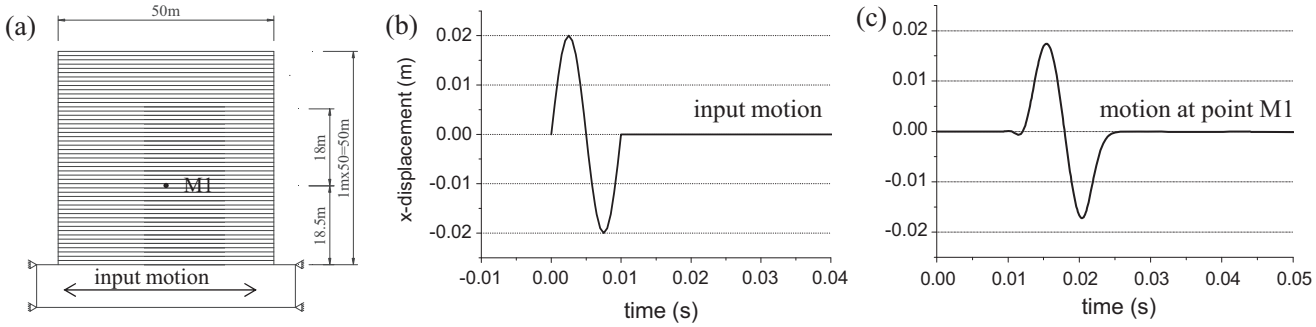

Fig. 9. Wave propagation through a stack of layers with DDA: (a) DDA model. (b) One-cycle sinusoidal incident wave time history used to induce vertical shear wave propagation in the DDA. (c) Wave forms as obtained with Discontinuous Deformation Analysis at point M1. After [48].

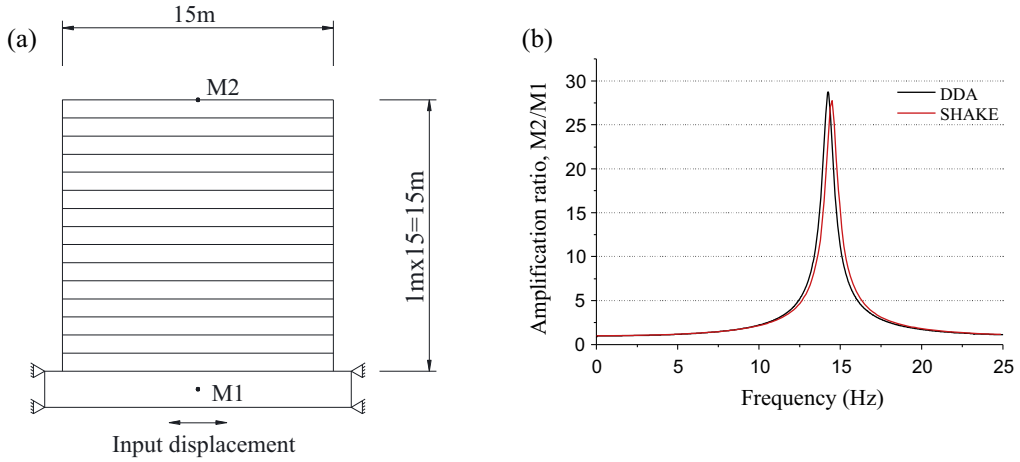

Fig. 10. (a) The model of the stacked layers in DDA. (b) Spectral ratios as obtained with DDA and SHAKE. After [48].

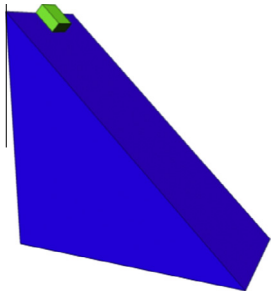

Fig. 11. The 3-D model used for the 3D-DDA verification of a block on an inclined plane.

Table 1
Numerical and physical parameters used in the first step of the verification study.

Parameter	Value
dd – dynamic parameter	1
*g*0 – normal contact spring stiffness	$4 * 10^8$ N/m
*g*1 – time step interval	0.001 s
*g*2 – maximum displacement ratio	0.001
density	2700 kg/m^3
Young's modulus	40 GPa
Poisson's ratio	0.18

through its base. Although in this paper we reviewed only verification studies, we choose to present this validation part, because the SHAKE program has been verified many times, its accuracy is well established for the underlying assumptions and boundary conditions, and validating the DDA with SHAKE for wave propagation applications seems to be an important step. Bao et al. [48] generated a stack of 15 layers in 2D-DDA, each with different mechanical properties (Fig. 10a), and applied a real earthquake time history at its base. They modeled the same sequence of layers in SHAKE, and compared the spectral amplifications obtained with the two approaches between the base and the top of the stack of layers. A very good agreement between the two methods was obtained (Fig. 10b), both for homogeneous and inhomogeneous media, both in the frequency and the amplitudes. Their results suggest the DDA can be used to model wave propagation through discontinuous media, provided that the numerical control parameters are well conditioned.

4. Benchmark tests for dynamic 3D-DDA

In this section we will review verification studies of 3D DDA, performed by the Rock Mechanics research group at the Ben-Gurion University of the Negev. Some verification studies have been published before, and are briefly reviewed, and some are presented here for the first time and are reviewed more thoroughly. Limitations of the current 3D-DDA code and formulation are discussed in Section 5.2.

4.1. Block sliding on an inclined plane – one direction of motion

The solution for a block sliding on an inclined plane was presented in Section 3.1.1. In this section an original verification

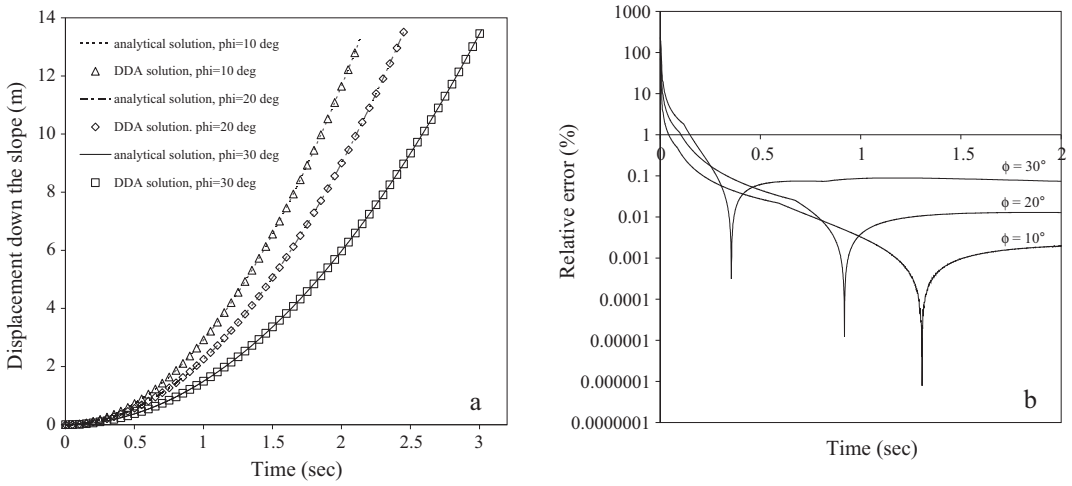

Fig. 12. (a) Downslope displacement histories of a block on an inclined plane subjected to gravity alone. Legend: curves – analytical solution, symbols – DDA solution. (b) The relative numerical error.

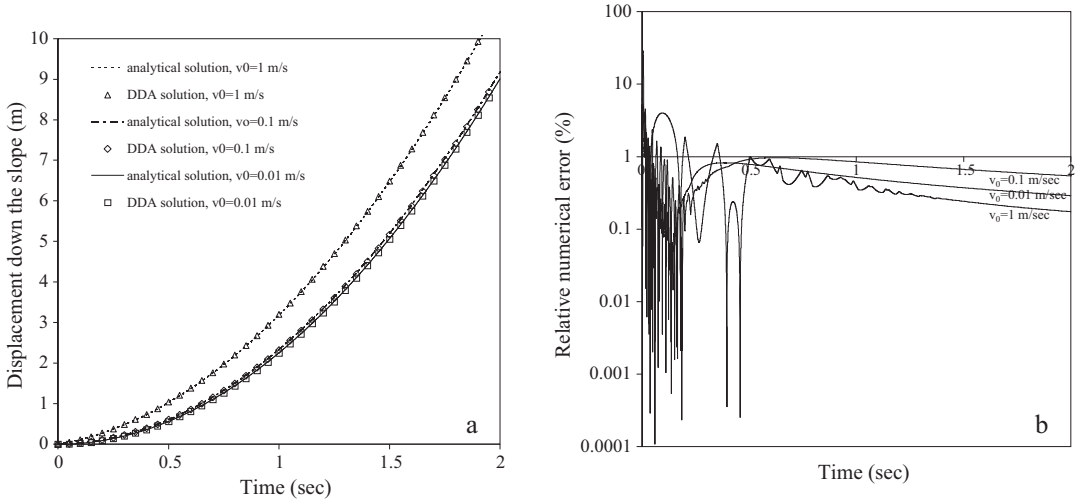

Fig. 13. (a) Downslope displacement histories of a block on an inclined plane subjected to gravity and different initial velocities. Legend: curves – analytical solution, symbols – DDA solution. (b) The relative numerical error.

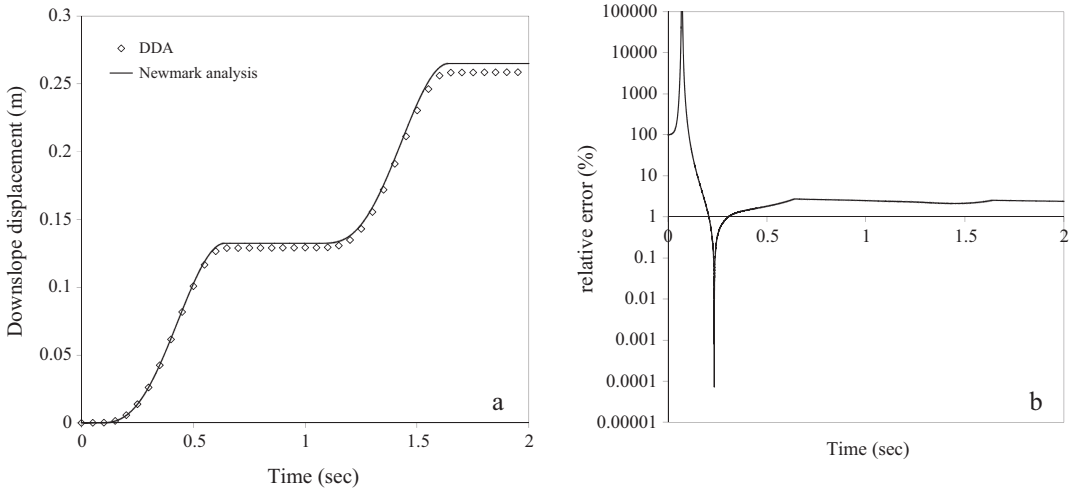

Fig. 14. (a) Downslope displacement histories of a block on an inclined plane subjected to gravity and 1-D sinusoidal input function. Legend: curve – analytical solution, symbols – DDA solution. (b) The relative numerical error.

study of the 3D-DDA is presented. The 3D-DDA mesh for the model of the block on an incline is constructed of a triangular prism base block, serving as the incline, with height of 10 m, inclination angle of $\alpha = 45°$ and depth of 5 m. The sliding block is a box, with dimensions 1 m × 1 m × 0.5 m (see Fig. 11). The base block is fixed in space, and the sliding block is loaded by two loading points, for the third step of the verification study, as explained below.

This verification study of the block on an incline is performed in three steps: first the response of the block when subjected to gravity, starting at rest, is examined, then the block is given initial horizontal velocity, and finally the block is subjected to one-dimensional horizontal sinusoidal acceleration. When subjecting the 3D block to initial velocity and acceleration in one direction only, the problem is basically reduced to a 2D problem, similar to the one presented in Section 3.1.1.

4.1.1. Block starting at rest

In this step the block is subjected to gravity alone ($A = 0$), starting at rest ($\dot{d}_0 = 0, d_0 = 0$). In this case, Eq. (8) becomes:

$$d(t) = \frac{1}{2}g(\sin\alpha - \cos\alpha\tan\phi)t^2 \tag{14}$$

The numerical and physical parameters used are listed in Table 1.

The downslope displacement history is compared for three values of friction angle: 10°, 20° and 30° (remembering the inclination angle of the slope is 45°). In Fig. 12a the results of the first step of the verification study are presented. Note the excellent agreement between the analytical and numerical solutions. In Fig. 12b the relative numerical error, defined earlier in Eq. (9) is presented. After 0.2 s the numerical error drops to below 1%, demonstrating the excellent agreement between the two solutions.

4.1.2. Block starting with initial velocity

The next step of the verification study is applying initial velocity $\dot{d}_0$ to the sliding block, and comparing the downslope displacements of the block to the ones computed by the analytical solution. In this case, where no external forces are applied on the block, Eq. (8) becomes:

$$d(t) = \frac{1}{2}g(\sin\alpha - \cos\alpha\tan\phi)t^2 + \dot{d}_0 t \tag{15}$$

In this verification step the numerical and physical parameters remain identical to the values presented in Table 1, except for the time step interval that is reduced to 0.0001 s.

The initial velocities are applied horizontally in the dip direction at three different values: 0.01, 0.1 and 1 m/s. Results for downslope displacement histories are presented in Fig. 13a. The agreement between the analytical and the numerical solutions is good for all three different velocities, as demonstrated by the relative numerical error plotted in Fig. 13b: less than 1% after 0.5 s of the analysis.

4.1.3. Block subjected to sinusoidal acceleration input

The third step of the verification study is comparing the downslope displacements of the block computed by an analytical solution, with those obtained by the 3D-DDA, where the sliding block is subjected to a one-dimensional horizontal sinusoidal acceleration, as in Fig. 1. The amplitude and frequency used for the input acceleration are 2 m/s^2 and 1 Hz, respectively.

Here the 'Newmark' type analysis is used as the analytical solution, as in the 2D-DDA verification explained earlier in Section 3.1.1. The friction angle of the interface between the slope and the sliding block is set to $\phi = 50°$, higher than the inclination angle $\alpha = 45°$, so block sliding will initiate only when the yield acceleration is exceeded. The numerical and physical parameters are identical to the ones listed in Table 1, except for a reduced time step size of 0.0001 s and the normal contact spring stiffness of $7 * 10^9$ N/m.

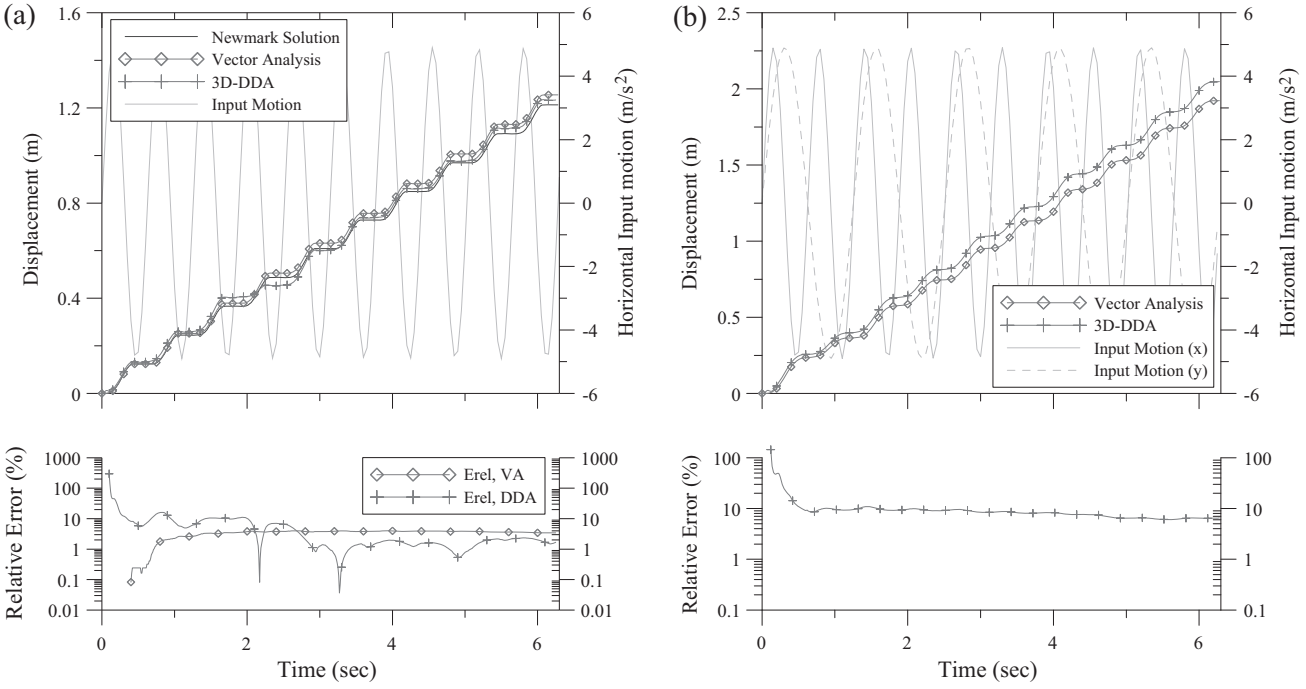

Fig. 15. Block displacement vs. time for the case of a block on an incline subjected to gravitational and cycles of horizontal sinusoidal loading. (a) Comparison between the Newmark solution, VA and 3D-DDA for 1D horizontal input motion along the *X* axis. The relative error for the numerical solutions is plotted in the lower panel where the Newmark solution is used as a reference. (b) Comparison between VA and 3D-DDA for 2D horizontal input motion along the *X* and *Y* axes simultaneously. The relative error is plotted in the lower panel where the VA is used as a reference. From [51].

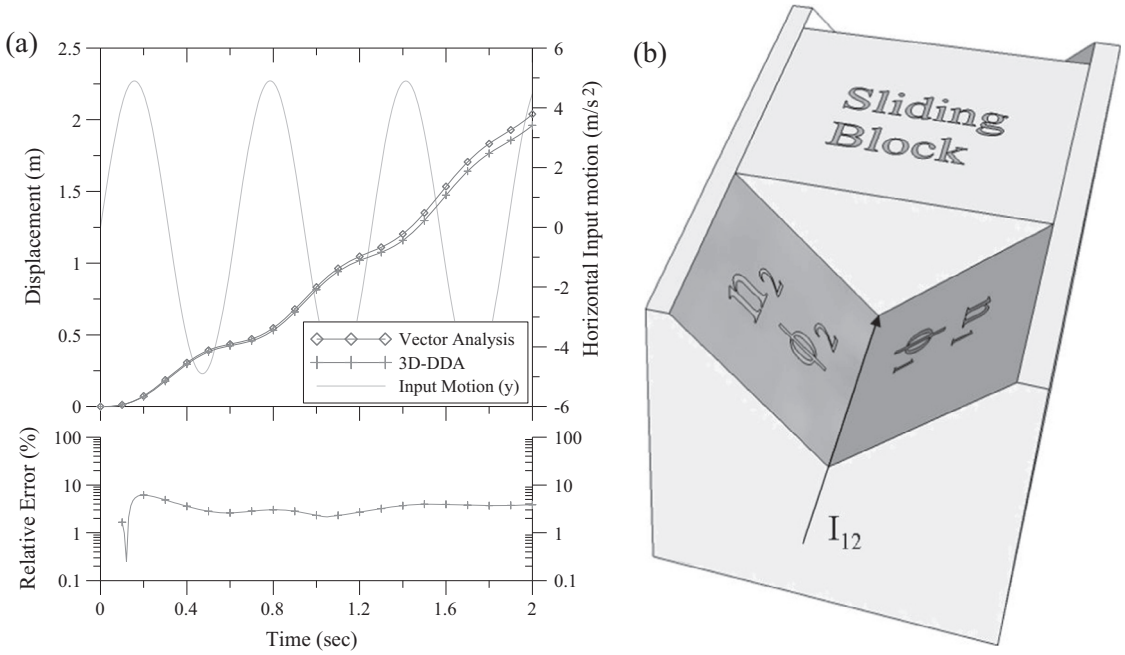

Fig. 16. Dynamic sliding of a wedge: comparison between 3D-DDA and VA solutions. (a) Wedge response to one component of horizontal sinusoidal input motion and self weight. Lower panel presents the relative error. (b) The wedge model in the 3D-DDA. From [51].

In Fig. 14a the downslope displacement histories calculated by the Newmark analysis and the 3D-DDA code are presented. The agreement between the two is good, and can again be expressed in terms of relative error, presented in Fig. 14b. During most of the analysis the error remains below 3%.

4.2. Block sliding on an incline – loading in two directions

Bakun-Mazor et al. [51,52] have derived a semi-analytical 3D-formulation for solving dynamic three dimensional displacements of single and double plane sliding (Section 4.4). In their paper, Bakun-Mazor et al.[51] presented an analytical formulation which they called Vector Analysis (VA), based on the limiting equilibrium equations of vector forces acting on a block on an inclined plane. The dynamic equations of motion of their analytical solution have a discrete nature, therefore the solution is considered semi-analytical. The formulation is explained in details in [51,52]. They first verified their new formulation with the Newmark type analysis for a block subjected to horizontal harmonic external force in the dip direction, as explained earlier, and once their new method proved valid, they compared the 3D-DDA numerical results to the results they obtained with their 3D-analytical solution. They subjected the block to sinusoidal accelerations in the horizontal dip and strike directions, with different amplitudes and frequencies, and obtained a good agreement, where the numerical error in the final position of the block after 6 s was approximately 8% (Fig. 15).

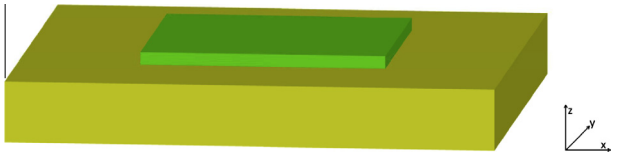

Fig. 17. The 3D model used in the verification study for block response to shaking foundation. The lower yellow block is displaced by the time-dependent displacement vector, and the displacements of the green, upper, responding block are measured. (For interpretation of the references to color in this figure legend, the reader is referred to the web version of this article.)

4.3. Failure mode mapping for the block on an incline problem

As previously reviewed in Section 3.2, a block on an incline has four possible modes (see Fig. 4). In this section the verification of 3D-DDA with the failure mode chart is reviewed.

4.3.1. Gravitational loading

Since the 3D-DDA has not been verified many times in the past, Yagoda-Biran and Hatzor [43] first verified the 3D-DDA with the previously published failure mode chart as derived by [39–42], using the same criteria for determining the first motion of the block as used for the 2D comparison discussed in Section 3.2. The range for α was between 14° and 50°, ϕ was 20° in most of the simulations, and δ was between 11° and 50°. An excellent agreement was obtained between the two solutions; 49 out of the 51 DDA simulations produced the failure mode predicted by the analytical mode chart.

4.3.2. Pseudo-static loading

After verifying the 3D-DDA with the original failure mode chart for gravitational loading, Yagoda-Biran and Hatzor [43] proceeded with comparing the 3D-DDA and their newly developed mode chart incorporating a pseudo-static force, using the same criteria for determining the first motion of the block as used for the 2D comparison. The slope angle α used was 10° for most of the simulations. The block slenderness range δ was between 6° and 70°, and the range of input friction angle ϕ between 6° and 80°. The change in the angle ψ was controlled by changing the magnitude of the applied pseudo-static force. All 89 simulations performed with the 3D-DDA returned failure modes as predicted by the analytical mode chart.

4.4. Sliding of a tetrahedral wedge

Bakun-Mazor et al. [51] verified the 3D-DDA with a semi analytical solution for a classic problem in rock mechanics – the wedge failure (double face sliding, Fig. 16b). There is no analytical solution describing the dynamic sliding of a wedge, therefore Bakun-Mazor

Table 2
Physical and numerical control parameters used in the verification study of the responding block.

Parameter	Value
dd – dynamic parameter	1 (fully dynamic)
*g*0 – normal contact spring stiffness	$1 * 10^9$ N/m
*g*1 – time step size	0.0001 s
*g*2 – maximum displacement ratio	0.001
density	2250 kg/m^3
Young's modulus	17 GPa
Poisson's ratio	0.22

et al. [51] compared the Vector Analysis (VA) semi-analytical formulation, described briefly in Section 4.2, with the numerical 3D-DDA for the case of a wedge. The input acceleration to the wedge was a sine function acting parallel to the line of intersection between the boundary planes along which the wedge slides. The plunge of the line of intersection was 30° below the horizon, and the friction of the sliding interfaces was set to 20°. They obtained a good agreement between the 3D-DDA and their newly developed analytical formulation where the relative numerical error remained below 7% for the entire simulation (Fig. 16a).

4.5. Block response to induced displacement in the foundation

A verification of the case of a responding block to moving foundation in three dimensions using 3D-DDA is presented here for the first time. This verification is based on the one-dimensional verification described in Section 3.4 by Kamai and Hatzor [34], with the exception that here the displacements, velocities and accelerations are now vectors.

4.5.1. The semi-analytical solution

The model used for the verification study is composed of two blocks (Fig. 17): a lower block subjected to time dependent displacements, and an upper block that responds to the displacements of the lower one. The dimensions of the blocks and their physical properties are irrelevant for the analytical solution, since it only considers the friction coefficient, as shown below. For the 3D-DDA, though, block dimensions and properties are of importance. Each of the two blocks, which are denoted from hereon 1 and 2 for the lower and upper blocks, respectively, has time dependent displacements $\bar{d}(t)$, velocities $\dot{\bar{d}}(t)$ and accelerations $\ddot{\bar{d}}(t)$.

The displacement induced to block 1, $\bar{d}_1$, is in the form of a cosine function:

$$\bar{d}_1(t) = \bar{A}(1 - \cos(2\pi\bar{f}t)) \tag{16}$$

where $\bar{A}$ and $\bar{f}$ are the amplitude and frequency of motion, respectively.

The forces acting on block 2 are its weight, m_2g, the normal from block 1, $N = m_2g$, and the frictional force between the two blocks, $\mu * m_2g$, where μ is the friction coefficient. Similarly to Eq. (14), Newton's second law of motion yields that the acceleration of block 2 is $\left|\ddot{\bar{d}}_2\right| = \mu * g$. Following Kamai and Hatzor [34], the direction of the frictional force, and therefore of $\ddot{\bar{d}}_2$, is determined by the direction of the relative velocity between the two blocks, $\dot{\bar{d}}^* \equiv \dot{\bar{d}}_1 - \dot{\bar{d}}_2$, defined by the unit vector of the relative velocity, $\hat{\dot{d}}^*$.

When $\left|\dot{\bar{d}}^*\right| = 0$, the acceleration of block 2 ($\ddot{\bar{d}}_2$) is determined by the acceleration of block 1 ($\ddot{\bar{d}}_1$). When the acceleration of block 1 exceeds the yield acceleration $\mu * g$, over which block 2 no longer moves in harmony with block 1, the frictional force direction is determined by the direction of $\hat{\dot{d}}^*$, but the magnitude of $\ddot{\bar{d}}_2$ is equal to $\mu * g$. This rationale can be formulated as follows:

$$\begin{aligned} &\text{If } \left|\dot{\bar{d}}^*\right| = 0 \quad \text{and} \quad \left|\ddot{\bar{d}}_1\right| \leqslant \mu \cdot g \quad \text{then} \quad \ddot{\bar{d}}_2 = \ddot{\bar{d}}_1 \\ &\qquad\qquad \text{and} \quad \left|\ddot{\bar{d}}_1\right| > \mu \cdot g \quad \text{then} \quad \ddot{\bar{d}}_2 = (\mu \cdot g) \cdot \hat{\ddot{d}}_1 \\ &\text{If } \left|\dot{\bar{d}}^*\right| \neq 0 \qquad\qquad \text{then} \quad \ddot{\bar{d}}_2 = (\mu \cdot g) \cdot \hat{\dot{d}}^* \end{aligned} \tag{17}$$

This set of conditions and inequalities was applied using a MATLAB script, with a time step of 0.0001 s. Since the analytical solution is calculated numerically, it is actually a semi-analytical solution.

4.5.2. The numerical model

The actual model used for the 3D-DDA is shown in Fig. 17. The dimensions of block 1 are 4 m × 4 m × 0.5 m, and the dimensions of block 2 are 2 m × 2 m × 0.1 m. Block 2 was designed to be very flat, so as to avoid rotations during motion. The physical and numerical control parameters used in the verification analyses are listed in Table 2.

All numerical simulations lasted seven seconds of real time, where in the first two seconds no displacements were applied, allowing for gravity "turn-on" and settlement of the springs.

4.5.3. One direction of motion

The first step was inducing displacements to block 1 in the *x*-direction (see Fig. 17) only, similar to the work reported by Kamai and Hatzor [34], and comparing the 3D-DDA results to the semi-analytical solution presented here. This was done for three different cases:

(1) Constant amplitude (A) of 0.2 m and friction (μ) of 0.6, and changing frequency (f) (Fig. 18a).
(2) Constant f of 1 Hz and μ of 0.6, and changing A, (Fig. 19a).
(3) Constant f of 1 Hz and A of 0.5 m, and changing μ, Fig. 20a).

As can be observed from Fig. 18b, the relative error remains below 3% for most of the simulation time with frequencies of 2 and 3 Hz, and below 10% for frequency of 5 Hz. Generally, with increasing frequency the numerical error increases as well, as can be observed in Fig. 18b, where the numerical error for the simulation with frequency of 5 Hz increases with time.

In Fig. 19b the numerical error remains below 7% for amplitude of 0.3 m, and below 1% for amplitudes of 0.5 and 1 m for most of the simulation time. In Fig. 20b for friction coefficient of 1, the error remains below 7%, and for friction coefficients of 0.1 and 0.6 it remains below 1%.

4.5.4. Two directions of motion

In the second step of the verification study, displacements were induced to the lower block in the *x* and *y* directions (see Fig. 17), each with different amplitude and frequency. Results are presented in Figs. 21 and 22. In Fig. 21a the resultant horizontal displacement vs. time is presented, while Fig. 22 is a 3D plot of the *x* and *y* displacements vs. time, presented as the vertical axis. Again, the agreement between the 3D-DDA and the analytical solution is good, as expressed by the numerical error in Fig. 21b, which remains below 10% for the entire simulation. A deviation between the numerical and analytical solutions is observed with increasing simulation time (see Fig. 21).

4.5.5. Three directions of motion

The third verification step was subjecting block 1 to sinusoidal displacements in all three directions: *x*, *y* and *z*. Adding sinusoidal displacement in the *z* direction affects the response of block 2 as it

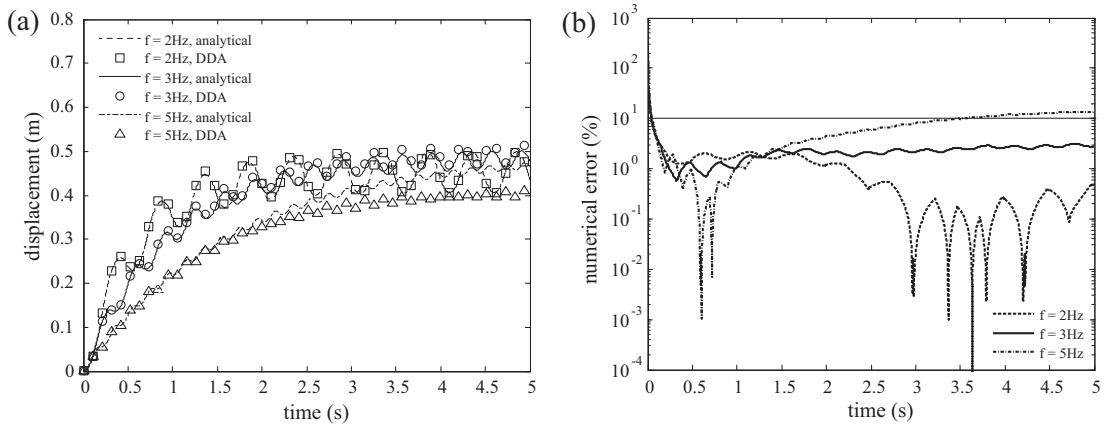

Fig. 18. (a) Comparison between the analytical solution (curves) and 3D-DDA solution (symbols). Amplitude of A = 0.2 m for the input motion and a friction coefficient of 0.6 remained unchanged, while input motion frequency changed. (b) relative numerical error, the 10% error is plotted for reference.

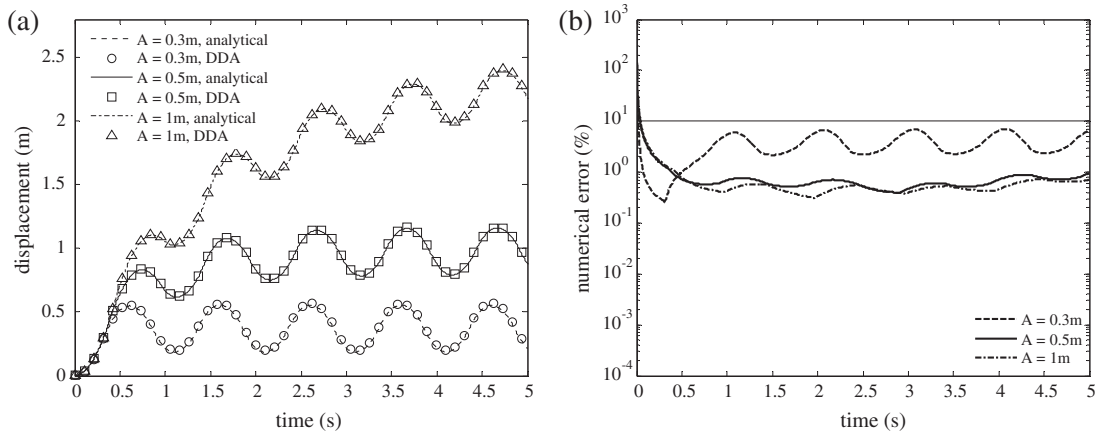

Fig. 19. (a) Comparison between the analytical solution (curves) and 3D-DDA solution (symbols). Frequency of 1 Hz for the input motion and a friction coefficient of 0.6 remained unchanged, while input motion amplitude changed. (b) Relative numerical error, the 10% error bar is plotted for reference.

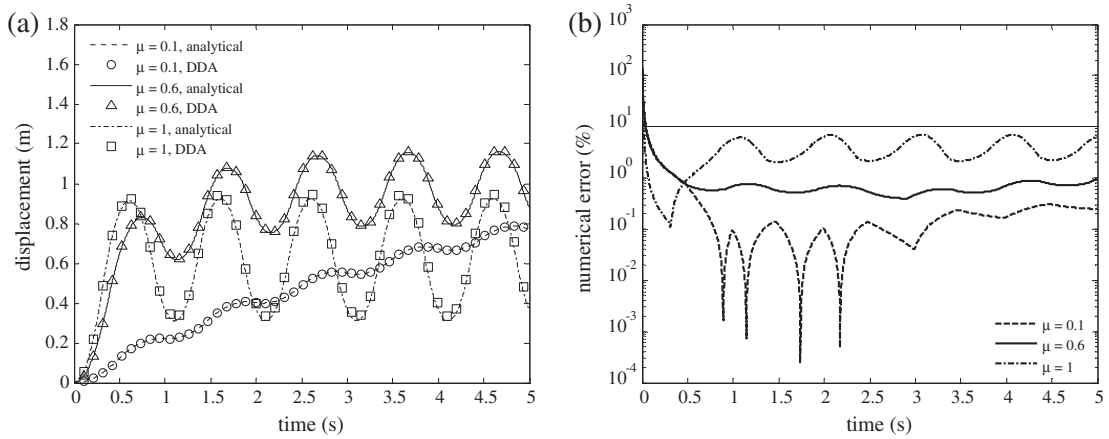

Fig. 20. (a) Comparison between the analytical solution (curves) and 3D-DDA solution (symbols). Frequency of 1 Hz and amplitude of 0.5 m for the input motion remained unchanged, while the friction coefficient changed. Notice the excellent agreement between the two solutions (b).

changes the normal force between the two blocks, and therefore the frictional force between them. This in turn changes the acceleration of block 2, $\ddot{\bar{d}}_2$, and yields a different displacement time history. Applying time-dependent displacements in the z direction is actually equivalent to time-dependent changes in g: when block 1 has positive z acceleration ($\ddot{d}_1\hat{k} > 0$), it is added to g. When $\ddot{d}_1\hat{k}$ is negative, it is subtracted from g. The analytical solution in this case assumes no other effect of the vertical displacement of block 1 on the horizontal displacement of block 2. The induced displacement function is now:

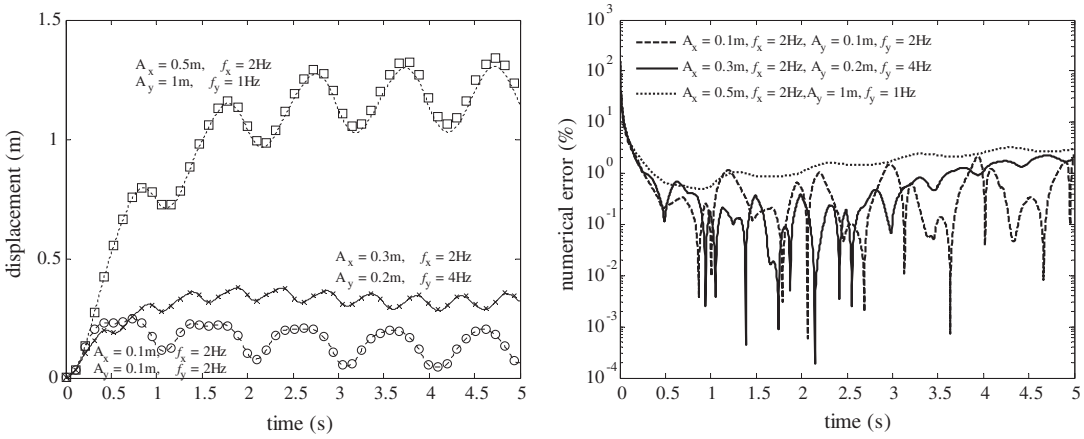

Fig. 21. Comparison between analytical (curves) and 3D-DDA (symbols) solutions. Each set of curves and symbols corresponds to a different set of amplitude and frequency for the input displacements, noted beside the data. Notice the excellent agreement between the two solutions.

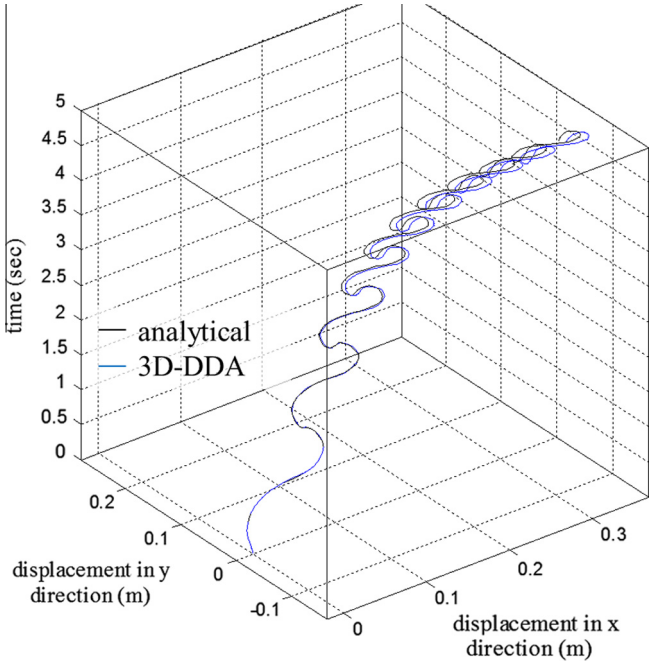

Fig. 22. Comparison between analytical (black curve) and 3D-DDA (blue curve) solutions. This analysis is for x amplitude and frequency of 0.3 m and 2 Hz and y amplitude and frequency of 0.2 m and 4 Hz, respectively. Notice the good agreement between the two solutions that decreases with analysis time. (For interpretation of the references to color in this figure legend, the reader is referred to the web version of this article.)

$$\bar{d}_1(t) = 0.1(1-\cos(2\pi 2t))\cdot\hat{i} + 0.1(1-\cos(2\pi 4t))\cdot\hat{j} + 0.1(1-\cos(2\pi t))\cdot\hat{k} \quad (18)$$

In Fig. 23 results of the verification study with three components of induced displacements are presented. Fig. 23a presents the resultant horizontal (x–y plane) displacement vs. time, for different values of the k – normal contact spring stiffness. The black heavy curve is the analytical solution, and the light colored curves are the 3D-DDA numerical solutions for different values of k. The range of contact spring stiffness that best fits the analytical solution is between $1*10^7$ and $1*10^9$ N/m, with stiffness of $k = 1*10^7$ N/m, or 0.0003 $E*L$, being the optimal selection, where E is the Young's modulus of the block and L is the length of the line across which the contact springs are attached. When considering 3D-DDA, it might be more relevant to compare k to $E*A$, where A is the area across which the contact springs are attached. In this case, $k = 1*10^7$ is ~0.0001 $E*A$, not much different from $E*L$. Fig. 23b demonstrates this with the relative numerical error. Note that for the results obtained with $k = 1*10^7$ N/m, the relative error stays below 3% for the entire analysis, and the error is well below 10% for $k = 1*10^8$ and $1*10^9$ N/m as well.

5. Discussion

5.1. Numerical control parameters

When running simulations with DDA there are several user-defined numerical control parameters the values of which have a significant effect on the results of the simulation. In this section we discuss these control parameters and suggest ways to make optimal selections. We would however like to stress that although some general guidance for optimal selection of the parameters is presented, given the effect they have on the results of the simulation, their calibration should be performed wherever possible, and routine sensitivity analyses are highly recommended.

5.1.1. Normal contact spring stiffness

The normal contact spring stiffness, k, is the stiffness of the virtual springs assigned at the dynamically formed contacts. In many sensitivity analyses it was found that the value of k significantly affects the results of the simulation.

Shi [53], in his user manual, recommended that as a rule of thumb $k = E*L$, where E is the Young's modulus of intact block material and L is the average block diameter. However, it is sometimes reported that the optimal value does not follow this rule. In their study of wave propagation with DDA Bao et al. [48] found that a k value lower by 1.5 orders of magnitude than Shi's rule of thumb is optimal. They suggested that the condition of the interface between the blocks might have an effect on the value selected: a weathered interface might effectively lower the Elastic modulus, therefore lower the optimal stiffness value. This observation is supported by Yagoda-Biran and Hatzor [45] who modeled a physical problem somewhat similar to the one modeled by Bao et al. [48] and concluded that a k value of about 2 orders of magnitude lower than Shi's rule of thumb [53] would be optimal. In other cases however, it seems that the optimal stiffness value even further deviates from Shi's rule of thumb, such as the case presented in Section 4.5.5. In this case, the optimal stiffness that results in the smallest numerical error is 2–4 orders of magnitude lower than

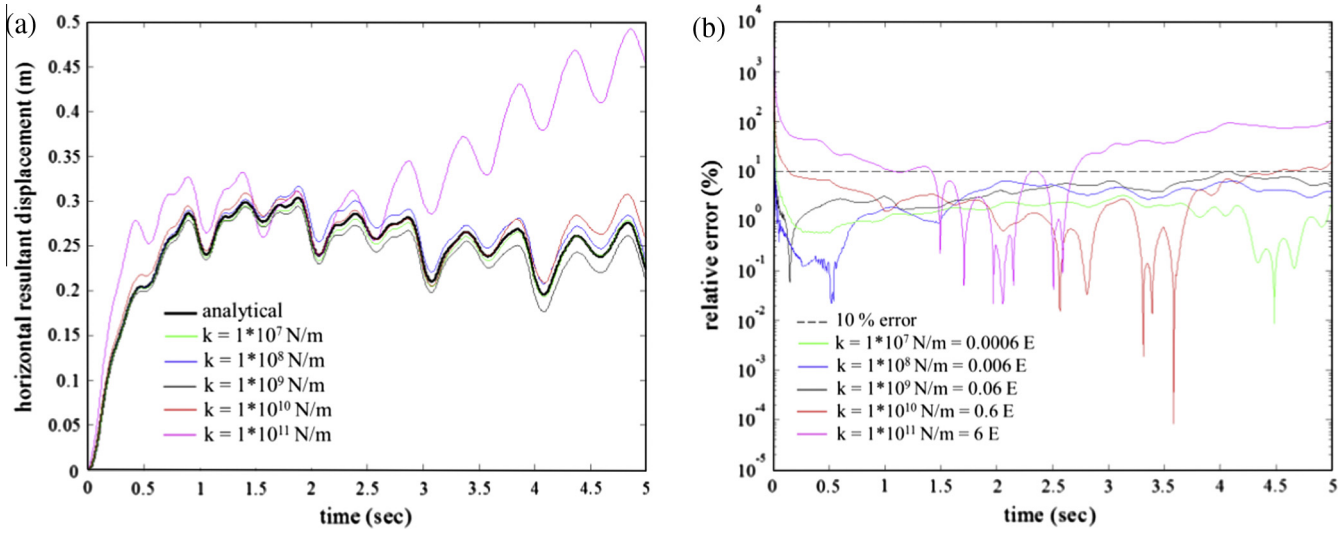

Fig. 23. (a) Comparison between analytical (black heavy curve) and 3D-DDA (light colorful curves) solutions. The best fit is obtained with contact spring stiffness of $k = 1 * 10^7$ N/m, but the overall trend of the analytical solution is maintained for all values of stiffness. (b) Relative numerical error for the different solutions presented in a. Note the black dashed line, indicating error of 10%. The green curve, representing contact spring stiffness of $1 * 10^7$ N/m, remains below 3% error the entire time span of the analysis, and is the best fit for this case. (For interpretation of the references to color in this figure legend, the reader is referred to the web version of this article.)

Shi's recommendation. In this case however the simulation is in 3D-DDA, while Shi's recommendations were given as a guide for 2D-DDA, therefore generalization might not be appropriate in this case.

5.1.2. Time step interval

Selecting an appropriate time step interval is an important issue with DDA simulations. When selecting a time step that is too long, the high frequency components are not resolved accurately enough. Time step intervals that are too short, on the other hand, result in long computation time, and may induce pseudo high frequency oscillations at the wave front [48].

As reviewed in [48], various authors proposed different rules of thumb for optimal time step size in relation to the wave period: less than 1% of the primary wave period in finite element simulations of nonlinear sound wave propagation [54], 5% of the shortest period of incident waves in Newmark time integration scheme [55], or smaller than $2/\pi$ of the un-damped period of vibration of the system described in Eq. (1), in order to avoid bifurcation in the DDA solution [32].

In order to ensure the stability of the numerical solution, the time step interval should be smaller than the fraction of the period that is equal to the ratio between the side length of the element along the direction of wave propagation path, and the wavelength, according to the Courant–Friedrichs–Levy condition [56]. This condition however does not ensure accuracy. In the next section we discuss how the choice of time step interval is reflected in the systems' damping.

5.1.3. Damping

In the original DDA code a damping submatrix was not incorporated in the equilibrium equations. Therefore, if the original code is to be used without modifications, damping can be introduced artificially by means of either kinetic damping or algorithmic damping. Kinetic damping is applied when the transferred velocity to the consecutive time step is reduced by some measure. Any value between 0 and 1 of the user defined dynamic control parameter would correspond to the percentage of velocity transferred from one time step to the following, that is, a dynamic parameter of 0.97 corresponds to 3% damping. When studying dynamic deformation of jointed rock slopes Hatzor et al. [57] reported that a 2% kinetic damping is required to obtain stable solution with the 2D-DDA version they used at that time. But if true and accurate displacements are required, then no kinetic damping should be introduced at all. This can be done provided that all other numerical control parameters are properly conditioned as discussed in Section 5.2.

Algorithmic damping [32] is associated with the time integration scheme used for integrating second order systems of equations over time. Numerical damping stabilizes the numerical integration scheme by damping out the unwanted high frequency modes. For the Newmark scheme used in DDA, it also affects the lower modes and reduces the accuracy of integration scheme to first order. In DDA, the numerical damping that is associated with the time integration scheme increases with increasing time step size. If the time step is small enough, the numerical damping phenomenon is insignificant. Bao et al. [48] suggested a way to utilize this time step size dependence of algorithmic damping, and obtained an equivalent damping ratio by seeking the time step size that will result in exactly the same damping ratio that would have been assumed otherwise in the structural analysis. They inspected the damped oscillations of the free end of a cantilever beam modeled with DDA with different time step intervals, and obtained an equivalent damping ratio, using the algorithmic damping in DDA as a function of time step interval. Then they modeled a stack of horizontal layers in DDA, subjected to earthquake displacements at the foundation, with a time step size of 0.001 s, which corresponded in that case to 2.3% damping. They compared the amplification and resonance frequency obtained with the DDA model, to those of an equivalent SHAKE [49,50] model with an input of 2.3% damping, and obtained an extremely good agreement between the two methods.

5.2. Limitations of 3D-DDA

5.2.1. Constructing a 3D-DDA mesh

Modeling three dimensional multi-block structures in 3D-DDA is an elaborate and challenging task. The block cutting code in 3D-DDA does not have a graphic interface, and does not accept three-dimensional blocks as input, but rather two-dimensional triangles, of which the blocks are built. For example, in order to build a rectangular face of a box, two triangles will be required, with

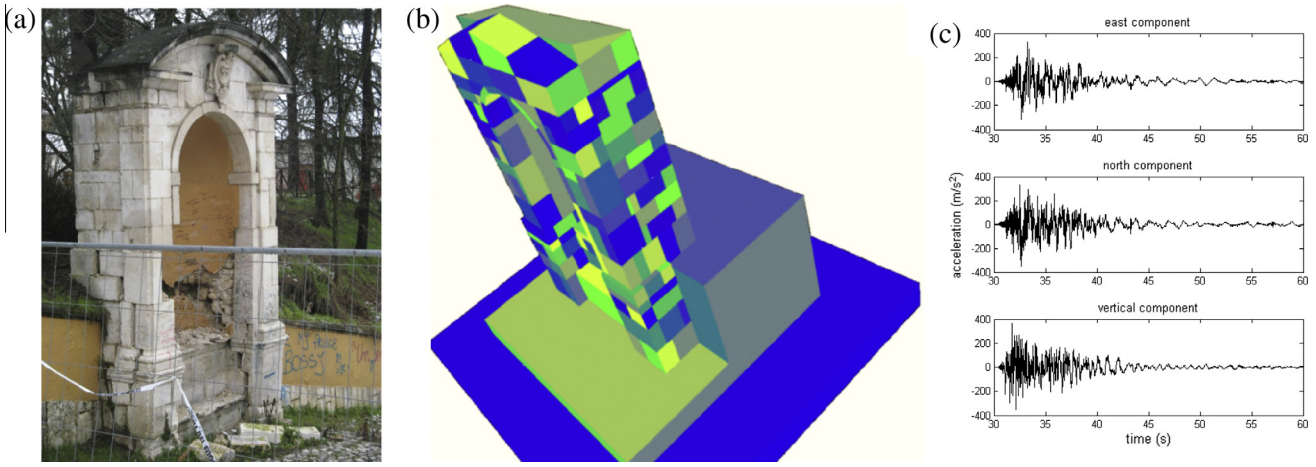

Fig. 24. (a) The masonry structure selected for 3D-DDA modeling in the city of L'Aquila, Italy. (b) Rotated view of the 3D-DDA model. (c) Acceleration time series from station AQK at L'Aquila.

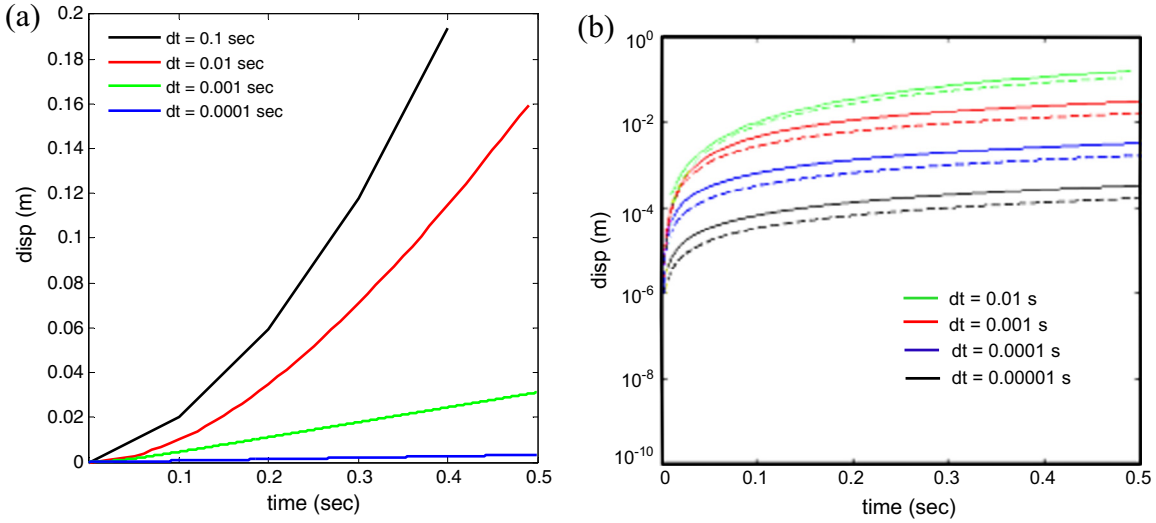

Fig. 25. Coupled effect of kinetic damping and time step size. (a) Cumulative displacement of a mass subjected to constant force, under 3% kinetic damping and different time steps, as calculated semi-analytically. (b) Displacements of a mass subjected to constant force and 3% kinetic damping computed with 3D-DDA (dashed lines) and with MATLAB (solid lines).

three vertices each. Therefore, to form a simple box, one needs to input the vertices for 12 triangles. When modeling problems involving only of a few blocks, the process of building the mesh might be tolerable, but when constructing meshes which consist of many blocks (see Section 5.2.2) the task becomes difficult and exhausting. It is therefore recommended to use computer aided design (CAD) software to construct a 3D DDA mesh, and use a function of the CAD software to export the model. In the work presented here in Section 5.2.2 we used the AutoCAD software. We built the model in the AutoCAD, exported the nodes to an Excel spreadsheet, and then used a MATLAB script to write the model's nodes to a file readable by the DDA. The scope of this paper does not allow for a full presentation of the process, but the interested reader is welcome to contact the corresponding author for more information.

5.2.2. The L'Aquila case study

The DDA in its two dimensional formulation has been used several times as a tool to estimate historical seismic hazard [34,45]. While attempting to use the 3D-DDA in a similar manner, we have stumbled upon limitations that suggest the 3D-DDA, at its current formulation, is still not ready for solving reliably dynamic problems involving a large number of blocks. We use the case study of L'Aquila to illustrate this problem,

The city of L'Aquila, the capital of the Abruzzo region, Italy, suffered strong ground motions during the earthquake of April 6, 2009. Over 300 people were killed, and many of the buildings in the old city were severely damaged and evacuated. Since there are several strong ground motion accelerographs at and near the city, this seemed as an excellent case study to check the validity of the DDA for solving complicated dynamic problems in three dimensions.

We searched the old city of L'Aquila for small, simple buildings that can be easily modeled with the 3D-DDA. We found a small masonry structure that was damaged by the earthquake, but did not collapse (Fig. 24a). Naturally, the observed damage cannot be modeled correctly with 2D-DDA, and a 3D approach is required. The model of the structure in 3D-DDA was comprised of 197 blocks, and is presented in Fig. 24b.

When trying to run forward analyses with the model, subjecting it to the acceleration time series as recorded in station AQK (Fig. 24c) located some 500 m away from the structure, the

solution converged only when kinetic damping of at least 3% was used, that is, dynamic parameter $\leqslant 0.97$, and a time step size no larger than 0.00001 s. With less kinetic damping and longer time step sizes we were not able to obtain stable solutions. We believe the necessity to introduce kinetic damping and extremely small time steps results from limitations of the contact algorithm in its current form that does not allow the system to converge when a large number of contacts must be solved in each and every iteration. The choice of such a small time step inevitably leads to extremely long CPU time, especially when running simulations with long "real" run time of tens of seconds. The use of small time step intervals in the 3D-DDA, smaller than the ones used in similar simulations in 2D-DDA, was observed many times. For example, the 3D simulations in [43] used a time step size two orders of magnitude smaller than the time step size used in similar 2D-DDA simulations. For the case of the responding block to induced displacements, the time step size used in the 3D-DDA case in Section 4.5 is one order of magnitude smaller than the 2D-DDA case in Section 3.4 [35]. For the case of a block on an incline, the time step size used in the 2D-DDA case is 0.002 s [34], while the 3D-DDA simulation in Section 4.1 used a time step size of 0.0001 s.

Furthermore, we noticed that the displacements of the blocks were several orders of magnitude smaller than expected. These results led us to investigate what effect does the coupling of kinetic damping and small time step has on the numerically obtained cumulative displacements. We conducted a numerical experiment, using MATLAB, where the time dependent displacements of a mass driven by a constant force were computed, with kinetic damping of 3% and different time step sizes. As observed in Fig. 25a, when using kinetic damping, the cumulative displacement decreases with decreasing time step, an effect also observed in the same experiment performed with the 3D-DDA (Fig. 25b). This effect was not observed when no kinetic damping was applied: the time step size had no effect on the cumulative displacements. Furthermore, decreasing the kinetic damping by even 2%, down to 1% damping, did not change the results significantly: the displacements were still highly restrained.

To summarize, the combination of a very small time step interval and kinetic damping of a small percentage significantly decreases the cumulative displacement during the simulation rendering the numerical results inaccurate and unrealistic. It is also evident that a small increase in kinetic damping coefficient will not make a great difference when very small time steps are used. Ideally, it would be preferable to use zero kinetic damping in dynamic DDA simulations, as the displacements per time step are reduced with increasing time step size anyhow due to the inherent algorithmic damping in DDA.

In cases such as these, where displacements are the desirable output, these limitations of the current version of the 3D-DDA code are not tolerable, and this effect makes the 3D-DDA, in its current form, inapplicable for dynamic simulations of multi-block systems. A new contact algorithm has been introduces by Shi [58], but has not yet been implemented in executable codes. After the new contact algorithm is implemented 3D-DDA should be tested again for its applicability for multi-block systems and multiple contacts.

6. Summary and conclusions

In this paper the validity of dynamic analysis with 2D and 3D DDA is verified by reviewing previously published verification studies as well as presenting newly developed, original verifications, all of which have been developed by the rock mechanics research group at Ben-Gurion University of the Negev. As the numerical discrete element DDA method is becoming more popular in rock mechanics and engineering geology research it becomes supremely important to verify the accuracy and applicability of the method before it is accepted and established as a standard analytical approach in the practice. The DDA has been proven to accurately solve problems involving block translations (block on an incline, double face sliding) and rotations (rocking of a free standing column) when the loading is applied at the center of the block, as well as translations when the loading is applied at the foundation (responding block). It has been proven to accurately solve large displacements, as well as wave propagation problems, that involve small displacements, despite the simply deformable blocks assumption and the first order approximations. It is suggested here, however, that future research should be invested in testing the accuracy of DDA in capturing site response for more complex geometries and configurations than reviewed here, because the potential of this method is vast.

The accuracy of the DDA highly depends on an educated selection of the numerical control parameters, first and foremost the penalty parameter otherwise known as the contact spring stiffness, as well as the time step size. A wise selection of the time step size would balance between small computation times and high accuracy. A wise contact spring stiffness selection would ensure accuracy of the solution; the block size becomes an issue primarily when dealing with wave propagation problems.

Naturally, 2D-DDA cannot be used in cases where out-of-plane deformations are expected in the physical problem. In such cases using the 3D-DDA would seem more appropriate although as much as we have experimented with 3D-DDA in its current formulation we have concluded that obtaining a stable solution to dynamic problems involving a large number of blocks is a very challenging task.

It is suggested here that the verifications reported in this paper would be performed for every modification made to DDA or any other numerical discrete element code.

Acknowledgements

We thank the editor, Prof. Vaughan Griffiths, and three anonymous reviewers for valuable comments, which greatly improved the quality of the manuscript. We thank Dr. Gen-hua Shi for access to most updated version of 2D and 3D DDA codes, ongoing code modifications, and stimulating discussions. We also thank Drs. Ronnie Kamai, Dagan Bakun-Mazor and Huirong Bao for their friendship, collaboration, stimulating discussions and willingness to share results. The original sections of this study were funded by Israel Science Foundation through Grant ISF-2201, Contract No. 556/08.

References

[1] Shi G-H. Discontinuous Deformation Analysis – A New Numerical Method for the Statics and Dynamics of Block System [Ph.D. Thesis]. Berkeley, University of California: Berkeley; 1988.
[2] Shi G-h, Goodman RE. Generalization of two dimensional discontinuous deformation analysis for forward modeling. Int J Numer Anal Meth Geomech 1989;13:359–80.
[3] G-h Shi. Block system modeling by discontinuous deformation analysis. Southampton, UK: Computational Mechanics Publication; 1993.
[4] Shi G-h, Goodman RE. Two dimensional discontinuous deformation analysis. Int J Numer Anal Meth. Geomech 1985;9:541–56.
[5] Shi G-h. Three dimensional discontinuous deformation analyses. In: Proceedings of the 38th US Rock Mechanics Symposium. Washington, DC2001. p. 1421–8.
[6] Jing L. Formulation of discontinuous deformation analysis (DDA) – an implicit discrete element model for block systems. Eng Geol 1998;49(3–4):371–81.
[7] Jing L. A review of techniques, advances and outstanding issues in numerical modeling for rock mechanics and rock engineering. Int J Rock Mech Min Sci 2003;40:283–353.
[8] Jing L, Hudson JA. Numerical methods in rock mechanics. Int J Rock Mech Min Sci 2002;39(4):409–27.
[9] Jing L, Stephansson O. Fundamentals of discrete element methods for rock engineering: theory and applications. Amsterdam: Elsevier; 2007.

[10] MacLaughlin MM, Doolin DM. Review of validation of the discontinuous deformation analysis (DDA) method. Int J Numer Anal Meth Geomech 2006;30(4):271–305.
[11] Lin CT, Amadei B, Jung J, Dwyer J. Extension of discontinuous deformation analysis for jointed rock masses. Int J Rock Mech Min Sci Geomech Abstr 1996;33:671–94.
[12] Ning YJ, Yang J, Ma GW, Chen PW. Contact algorithm modification of DDA and its verification. In: Ma G, Zhou Y, editors. Analysis of discontinuous deformation: new developments and applications; 2010. p. 73–81.
[13] Bao HR, Zhao ZY. An alternative scheme for the corner-corner contact in the two-dimensional Discontinuous Deformation Analysis. Adv Eng Softw 2010;41(2):206–12.
[14] Bao HR, Zhao ZY. The vertex-to-vertex contact analysis in the two-dimensional discontinuous deformation analysis. Adv Eng Softw 2012;45(1):1–10.
[15] Shi G-H. The numerical manifold method and simplex integration. Vicksburg. MS: US Army Corps of Engineers: Waterways Experiment Station; 1997.
[16] Bao HR, Zhao ZY. Modeling brittle fracture with the nodal-based Discontinuous Deformation Analysis. Int J Comp Meth 2013;10(6):55.
[17] Jiao YY, Zhang XL, Zhao J. Two-dimensional DDA contact constitutive model for simulating rock fragmentation. J Eng Mech-Asce 2012;138(2):199–209.
[18] Grayeli R, Mortazavi A. Discontinuous deformation analysis with second-order finite element meshed block. Int J Numer Anal Meth Geomech 2006;30:1545–61.
[19] Jiao YY, Zhang XL, Zhao J, Liu QS. Viscous boundary of DDA for modeling stress wave propagation in jointed rock. Int J Rock Mech Min Sci 2007;44(7):1070–6.
[20] Bao HR, Hatzor YH, Huang X. A new viscous boundary condition in the two-dimensional discontinuous deformation analysis method for wave propagation problems. Rock Mech Rock Eng 2012;45(5):919–28.
[21] Mikola RG, Sitar N. Explicit three dimensional Discontinuous Deformation Analysis for blocky system 47th US rock mechanics/geomechanics symposium. San Francisco: American Rock Mechanics Association; 2013.
[22] Kim Y, Amadei B, Pan E. Modelling the effect of water, excavation sequence and rock reinforcement with discontinuous deformation analysis. Int J Rock Mech Min Sci Geomech Abstr 1999;36:949–70.
[23] Jing L, Ma Y, Fang Z. Modeling of fluid flow and solid deformation for fractured rocks with discontinuous deformation analysis (DDA) method. Int J Rock Mech Min Sci Geomech Abstr 2001;38:343–55.
[24] Chen HM, Zhao ZY, Sun JP. Coupled hydro-mechanical model for fracture rock masses using the Discontinuous Deformation Analysis. Tunn Undergr Space Tech 2013;38:506–16.
[25] Ben YX, Xue J, Miao QH, Wang Y. Coupling fluid flow with discontinuous deformation analysis. In: Zhao J, Ohnishi Y, Zhao GF, editors. 10th international conference on advances in discontinuous numerical methods and applications in geomechanics and geoengineering (ICADD). Honolulu, HI; 2011. p. 107–12.
[26] Koyama T, Nishiyama S, Yang M, Ohnishi Y. Modeling the interaction between fluid flow and particle movement with discontinuous deformation analysis (DDA) method. Int J Numer Anal Meth Geomech 2011;35(1):1–20.
[27] Wu JH, Ohnishi Y, Nishiyama S. A development of the discontinuous deformation analysis for rock fall analysis. Int J Numer Anal Meth Geomech 2005;29(10):971–88.
[28] Moosavi M, Grayeli R. A model for cable bolt–rock mass interaction: integration with discontinuous deformation analysis (DDA) algorithm. Int J Rock Mech Min Sci 2006;43(4):661–70.
[29] Ning Y, Zhao Z. A detailed investigation of block dynamic sliding by the discontinuous deformation analysis. Int J Numer Anal Meth Geomech 2012;37:2373–93.
[30] MacLaughlin M, Sitar N, Doolin D, Abbot T. Investigation of slope-stability kinematics using discontinuous deformation analysis. Int J Rock Mech Min Sci 2001;38(5):753–62.
[31] Yeung MR. Analysis of three-hinged beam using DDA. In: Salami MR, Banks B, editors. Proceedings of the first international forum on discontinuous deformation analysis (DDA) and simulations of discontinuous media. Berkeley (CA): TSI Press; 1996. p. 462–9 [Albuquerque, NM].
[32] Doolin DM, Sitar N. Time integration in discontinuous deformation analysis. J Eng Mech ASCE 2004;130(3):249–58.
[33] Tsesarsky M, Hatzor YH, Sitar N. Dynamic displacement of a block on an inclined plane: analytical, experimental and DDA results. Rock Mech Rock Eng 2005;38(2):153–67.
[34] Kamai R, Hatzor YH. Numerical analysis of block stone displacements in ancient masonry structures: a new method to estimate historic ground motions. Int J Numer Anal Meth Geomech 2008;32:1321–40.
[35] Kamai R. Estimation of historical seismic ground-motions using back analysis of structural failures in archaeological sites, MSc thesis. Beer-Sheva: Ben-Gurion University of the Negev; 2006.
[36] MacLaughlin MM. Discontinuous deformation analysis of the kinematics of landslides. Berkeley: Department of Civil and Environment Engineering, University of California; 1997.
[37] Newmark N. Effects of earthquakes on dams and embankments. Geotechnique 1965;15(2):139–60.
[38] Goodman RE, Seed HB. Earthquake-induced displacements in sand embankments. J Soil Mech Found Div ASCE 1966;90(SM2):125–46.
[39] Ashby JP. Sliding and toppling modes of failure in models and jointed rock slopes. University of London, Imperial College; 1971.
[40] Bray JW, Goodman RE. The theory of base friction models. Int J Rock Mech Min Sci 1981;18:453–68.
[41] Hoek E, Bray JW. Rock slope engineering. 3rd revised ed. London: E & FN SPON; 1981.
[42] Yeung MR. Application of Shi's discontinuous deformation analysis to the study of rock behavior. Berkeley: University of California, Berkeley; 1991.
[43] Yagoda-Biran G, Hatzor YH. A new failure mode chart for toppling and sliding with consideration of earthquake inertia force. Int J Rock Mech Min Sci 2013;64:122–31.
[44] Makris N, Roussos YS. Rocking response of rigid blocks under near-source ground motions. Geotechnique 2000;50(3):243–62.
[45] Yagoda-Biran G, Hatzor YH. Constraining paleo PGA values by numerical analysis of overturned columns. Earthquake Eng Struct Dynam 2010;39:462–72.
[46] Ohnishi Y, Nishiyama S, Sasaki T, Nakai T. The application of DDA to practical rock engineering problems: issues and recent insights. In: Sitar MMAN, editor. Proceedings of the 7th international conference on the analysis of discontinuous deformation. Honolulu, Hawaii; 2005. p. 277–87.
[47] Yagoda G, Hatzor YH. Seismic risk estimation from overturning analysis of Hellenistic columns using DDA. In: Ju Y, Xisheng F, Bian H, editor. Proceedings of ICADD-8, the 8th international conference on the analysis of discontinuous deformation. Beijing, China; 2007. p. 123–8.
[48] Bao H, Yagoda-Biran G, Hatzor YH. Site response analysis with two-dimensional numerical discontinuous deformation analysis method. Earthquake Eng Struct Dynam 2014;43:225–46.
[49] Lysmer J, Seed HB, Schanable PB. SHAKE – A computer program for earthquake response analysis for horizontally layered sites. Berkeley; 1972.
[50] Schnabel PB, Lysmer J, Seed HB. SHAKE: A computer program for earthquake response analysis of horizontally layered sites. Berkeley: Earthquake Engineering Research Center, University of California; 1972. p. 102.
[51] Bakun-Mazor D, Hatzor YH, Glaser SD. 3D DDA vs analytical solutions for dynamic sliding of a tetrahedral wedge. In: Ma G, Zhou Y, editors. Proceedings of ICADD-9: the 9th international conference on analysis of discontinuous deformation. Singapore: Dover; 2009. p. 193–200.
[52] Bakun-Mazor D, Hatzor YH, Glaser SD. Dynamic sliding of tetrahedral wedge: The role of interface friction. Int J Numer Anal Meth Geomech 2012;36(3):327–43.
[53] Shi G-h. Discontinuous Deformation Analysis Programs, version 96, User's manual. In: Young RM-C, editor.1996.
[54] Kagawa Y, Tsuchiya T, Yamabuchi T, Kawabe H, Fujii T. Finite-element simulation of nonlinear sound-wave propagation. J Sound Vib 1992;154(1):125–45.
[55] Moser F, Jacobs LJ, Qu JM. Modeling elastic wave propagation in waveguides with the finite element method. NDT E Int 1999;32(4):225–34.
[56] Courant R, Friedrichs K, Lewy H. On the partial difference equations of mathematical physics. IBM J Res Develop 1967;11(2):215–34.
[57] Hatzor YH, Arzi AA, Zaslavsky Y, Shapira A. Dynamic stability analysis of jointed rock slopes using the DDA method: King Herod's Palace, Masada, Israel. Int J Rock Mech Min Sci 2004;41(5):813–32.
[58] Shi G. Basic theory of two dimensional and three dimensional contacts. In: Chen GQ, Ohnishi Y, Zheng L, Sasaki T, editors. ICADD-11: the 11th international conference on analysis of discontinuous deformation. Fukuoka (Japan) and London (UK): Taylor and Francis; 2013. p. 3–14.